



Original Article

Microstructural simulation of three-point bending test with pre-crack: Effect of sample size and loading configuration

Nuwong Chollacoop^{1*} and K. Sharvarn Kumar²

¹ National Metal and Materials Technology Center (MTEC),
Thailand Science Park, Khlong Luang, Pathum Thani, 12120 Thailand.

² Division of Engineering,
Brown University, Providence, RI 02912, USA.

Received 28 September 2007; Accepted 7 September 2008

Abstract

Deformation behavior in three-point bending test of Mo-Si-B alloy specimens with pre-crack was investigated by recourse to finite element analysis (FEA) with heterogeneous microstructures incorporated. The loading configuration was carried out by moving the top pin down, while the bottom pin remained fixed. The Mo-Si-B alloy consists of hard, brittle T2 (Mo_5SiB_2) phase embedded in a soft matrix of Mo solid solution. The sample contains pre-crack configuration at the middle in order to study the effect of the second phase (T2 particles) onto a crack tip during the bending test. Real optical micrographs were scanned, digitized, and meshed into a two dimensional model with constitutive relations of both phases. It was found that the plastic strain localization was not only caused by the hard T2 particles ahead of the crack tip, but also caused by the top pushing pin. This interaction between two strain fields was also observed if the microstructure were homogeneous. Two methodologies were explored in order to minimize this interaction in order to solely separate the effect of hard T2 particles ahead of the crack tip. The first one was to increase the distance between the top pin and the crack tip, while the second one was to approximate the pushing pin loading by end moment application. It was found that the strain interaction still appeared in both cases.

Keywords: finite element analysis, three-point bending, Mo-Si-B alloy, pre-crack

1. Introduction

For the high temperature application, Ni-based superalloys have been utilized for many years in the aerospace and aircraft industry. However, the limiting operating temperature for these alloys prompts for a search for a novice material, which can withstand a higher operating temperature to achieve a better fuel efficiency, especially for aircraft and aerospace applications. Over the past few decades, multiphase Nb- and Mo-based alloys have been the target of extensive research and development around the world since

they showed promising high temperature properties suitable for such applications. The complete overviews for both alloys are described elsewhere (Bewlay *et al.*, 2003; Dimiduk, 2003). Vigorous attempts have been dedicated to characterize their high-temperature properties, e.g. strength, toughness, and fatigue. Since experimental observation of high temperature test may sometimes be tedious or even impossible to be monitored at real-time, computational speculation based on experimental data offers useful insights and predicative abilities into the understanding of the mechanical properties of such alloys.

The present study is a follow-up to previous computational studies (Chollacoop *et al.*, 2006; Alur, 2007) in an attempt to explain the recrystallization behavior observed in the experiment of monotonic and cyclic loading at elevated

*Corresponding author.
Email address: nuwongc@mtec.or.th

temperature (Alur *et al.*, 2004). The current computational model focuses on the effects of the sample size and loading configuration onto the interaction of strain localization between crack tip and pushing pin in the three-point bending test simulation.

2. Computational modeling

The simulation approached chosen for the present study was a finite element analysis (FEA). Since the FEA investigation does not typically involve specific length scale, the present study needs further modification to the typical FEA by recourse to the incorporation of microstructural information. Figure 1 shows the schematic diagram of the methodology. First, the real micrograph was adjusted for the clear contrast between the two phases before being fed into an image processing tool. The image processor will then store an array of contrasts from each pixel in the micrograph so that the coordinate of the pixel and its contrasts are linked. This array is then fed into any generalized finite element analysis code in order to associate the contrast-coordinate array to the appropriate constitutive relations. Then, proper boundary condition and relevant FEA parameter are used as the input for the calculation.

Figure 2 shows the microstructure of Mo-Si-B alloy used in the present calculation with three levels of sample size, as indicated by the square boxes. This alloy consists of a hard, brittle phase (Mo_5SiB_2 or T2 shown as black islands in Figure 2) embedded in a soft matrix of Mo solid solution.

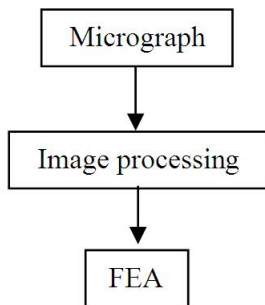


Figure 1. Schematic diagram of the microstructural finite element analysis.

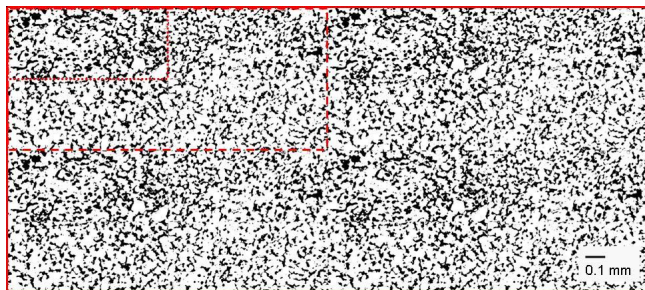


Figure 2. Three levels of microstructures used in the present calculation, as indicated by the square boxes.

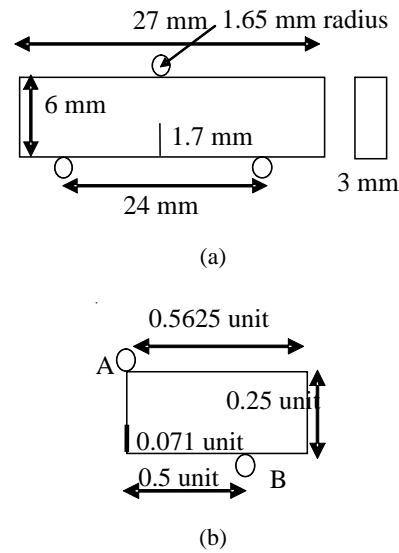


Figure 3: (a) Experimental configuration of the three-point bending test with (b) the half cell model for simulation due to the symmetry.

Note, that certain adjustment of the contrast/brightness of these two phases was already done in Figure 2 for the phase identification in the image processing stage.

According to Figure 1, each level of the micrograph was digitized by image analysis software into an array of 0 or 1, representing black or white pixel mapped over the coordinate of the micrograph. Then, this array was passed onto the finite element analysis code for further simulation.

Figure 3(a) depicts the experimental configuration with the sample length of 27 mm, height of 6 mm, and a thickness of 3 mm. The sample is sharply notched and compression-compression fatigue pre-cracked for the total pre-crack length of 1.7 mm (measured under optical microscope) at the center. The geometry of the notch and the minimum fatigue pre-crack length were according to ASTM E1820-01. The three-point bending test was set up on the universal testing machine in a vacuum at below 1.33×10^{-4} Pa with crosshead displacements of 10^{-3} and 10^{-5} mm/s.

For the three-point bending simulation with the test configuration shown in Figure 3(a), only half of the sample was modeled with the appropriate boundary condition and proper scaling with dimensional consistency (see Figure 3b). A commercially available FEA package (ABAQUS) was used to simulate the three-point bending by quasi-static displacement control of the top pin, while holding the bottom pin fixed. The top and bottom pins were approximated as rigid surfaces with frictionless interactions. Along the symmetrical line, the fatigue pre-crack was modeled as a mathematical sharp allowing only a vertical degree of freedom on the uncrack portion and an unconstrained deformation on the crack portion. No crack propagation was allowed in the present model. Since the sample thickness is half the sample height (3 mm), a plane strain element was used.

Both phases were assigned constitutive relations obtained from experimental observations at 1000K (Alur, 2004). In other words, the hard T2 phase was treated as being elastic with a Young's modulus of 383 GPa and a Poisson's ratio of 0.26 (Ito, 2001); whereas, the Mo matrix was treated as elastic-plastic with a Young's modulus of 324 GPa, a Poisson's ratio of 0.29, a yield strength of 400 MPa, and a linear work-hardening rate of 200 MPa per unit strain (Cheng *et al.*, 2001). Figures 4a-c show the FEA setup of

three levels of microstructures shown in Figure 2 covering $356 \times 800 \mu\text{m}^2$ (18,180 elements), $711 \times 1600 \mu\text{m}^2$ (72,900 elements), and $1,422 \times 3,200 \mu\text{m}^2$ (291,600 elements), respectively, all with an element size resolution of $2 \times 2 \mu\text{m}^2$.

3. Results and Discussion

The contour plots of plastic equivalent strain PEEQ (Figure 5a-c) were extracted from the simulation results of three levels of microstructures, as shown in Figures 4a-c. Since the sample sizes are not the same, appropriate comparison of strain localization was conducted at the scaled vertical displacement (U_2). In other words, the selected U_2 for Figure 5a is 0.05, that for Figure 5b is 0.1, and that of Figure 5c is 0.2, so that the degree of global rotational strain is comparable.

Since the hard T2 phase can only deform elastically, while soft Mo phase can accommodate plasticity, the high plastic strain deformation is observed in the T2 phase ahead

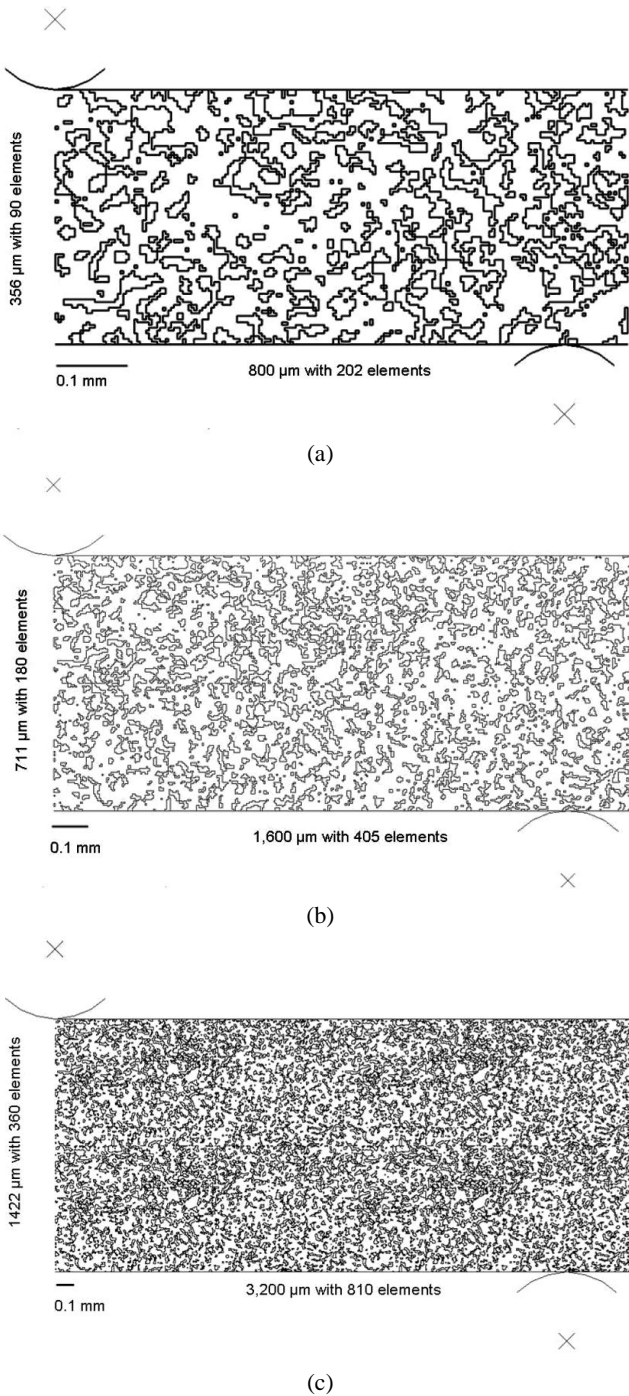


Figure 4. Finite element analysis models of the three levels of microstructures, (a) to (c), marked in Figure 2.

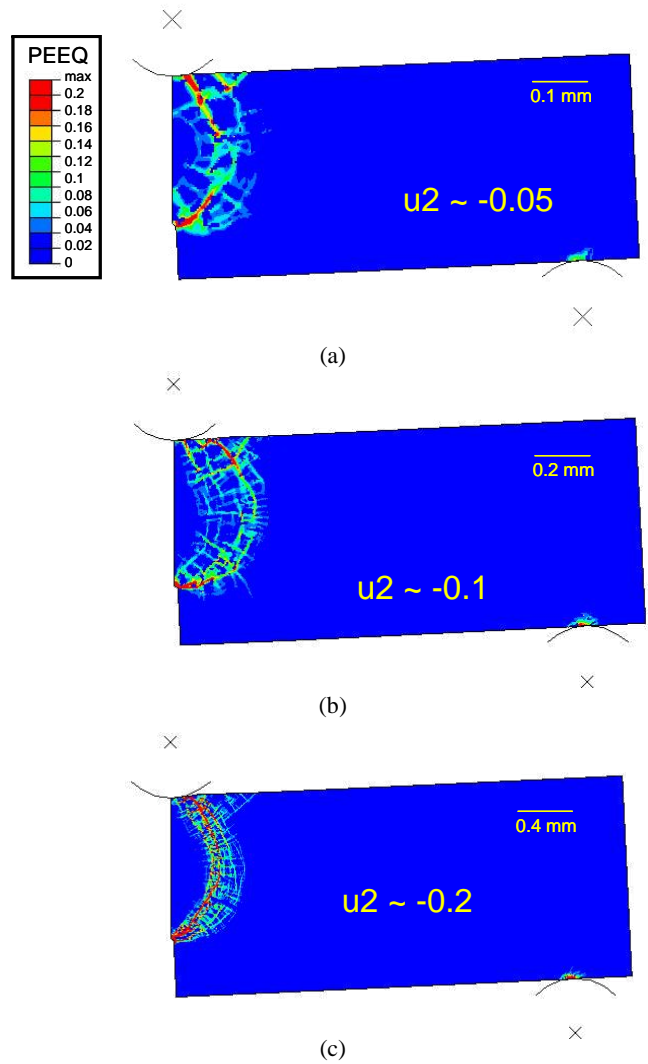


Figure 5. Contour plots of plastic equivalent strain for the three microstructures shown in Figures 4a-c at vertical displacement (U_2) of (a) 0.05, (b) 0.1 and, (c) 0.2.

of the crack tip with similar behavior observed directly underneath the loading top pin due to the indentation effect. Small plastic strain localization is also observed at the contact of the bottom fixed pin. It is obvious that the plastic strain localization ahead of the crack tip at the presence of the hard T2 particles is intervened by the plastic strain localization from the loading top pin. The degree of such intervention spans less area with larger distance between the crack tip and the top pin, as shown by the narrower colored regions in Figure 5a > Figure 5b > Figure 5c. However, the larger distance between the crack tip and the top pin seems to aggravate the narrow strain localization path, shown by a thin red line in Figure 5c. Hence, it is clear that the strain localization effect from both, the crack tip and the top pin, cannot be completely isolated by increasing the distance between them, so a careful interpretation of the plastic strain localization at the crack tip is required.

Another method to eliminate the indentation effect from the top pin was conducted by replacing the top/bottom pin configuration by the equivalent end moment application. The microstructure in Figure 4b was chosen for this investigation. The top pin was removed with the addition of the equivalent moment centered around the mid point of the sample right side. The contour plots of PEEQ for both loading configurations (pushing top pin vs. end moment application) were shown in Figure 6a-b at U2 of 0.035.

The change of loading configuration from pushing top pin to end moment application helps reducing the intervention between strain localizations from the contact point with the top pin and the crack tip. Figure 6b shows clearly the individual strain localization effect from either crack tip or

top bending, with the advent of strain localization region at the contact of the bottom fixed pin and the top right corner. However, with larger degree of three-point bending loading, the strain localization regions eventually connect, leading to the difficulty in solely isolating the strain localization effect from the crack tip. The early plastic strain localization can be investigated solely without any interference from the nature of the loading configuration.

4. Conclusions

Computation modeling of three-point bending of heterogeneous microstructures consisting of hard T2 particles embedded in a soft Mo matrix was conducted. Strain localizations were investigated based on differences in the constitutive relations of the two phases, especially the intervention from the top pushing pin to the crack tip. Two remedies were attempted by increasing the distance between them and changing the loading configuration from top pushing pin to end moment application. The larger distance between the top pushing pin and the crack tip merely lessens the area of intervention but with a greater strain localization connecting between the two sources. On the other hand, the end moment application can isolate the strain localization effect at the early stage of deformation (small degree of three-point bending) but with larger degree of bending, the strain localization regions were connected. Thus, the present study shows that careful interpretation of the strain localization at the crack tip in this heterogeneous microstructure is required for any meaningful observation.

Acknowledgements

NC would like to thank Dr. Anchalee Manonukul for her permission to use the ABAQUS license at MTEC.

References

- Alur, A.P., Chollacoop, N. and Kumar, K.S. 2004. High-temperature compression behavior of Mo-Si-B alloys. *Acta Materialia*. 52, 5571-5587.
- Alur, A.P., Chollacoop, N. and Kumar, K.S. 2007. Creep/Environment Effects on Crack Growth in a Mo-Si-B Alloy. *Acta Materialia*. 55, 961-974.
- Bewlay, B.P., Jackson, M.R. and Zhao, J.C. and Subramanian, P.R. 2003. Ultrahigh-Temperature Nb-Silicide-Based Composites. *MRS Bulletin*. 28, 646-653.
- Cheng, J., Nemat-Nasser, S. and Guo, W. 2001. A unified constitutive model for strain-rate and temperature dependent behavior of molybdenum. *Mechanics of Materials*. 33, 603-616.
- Chollacoop, N., Alur, A.P. and Kumar, K.S. 2006. Microstructural Simulation of Three-Point Bending Test with Mo-Si-B Alloy at High Temperature. *Proceedings of the Asian Symposium on Materials and Processing*, Bangkok, Thailand, November 9-10, 2006.

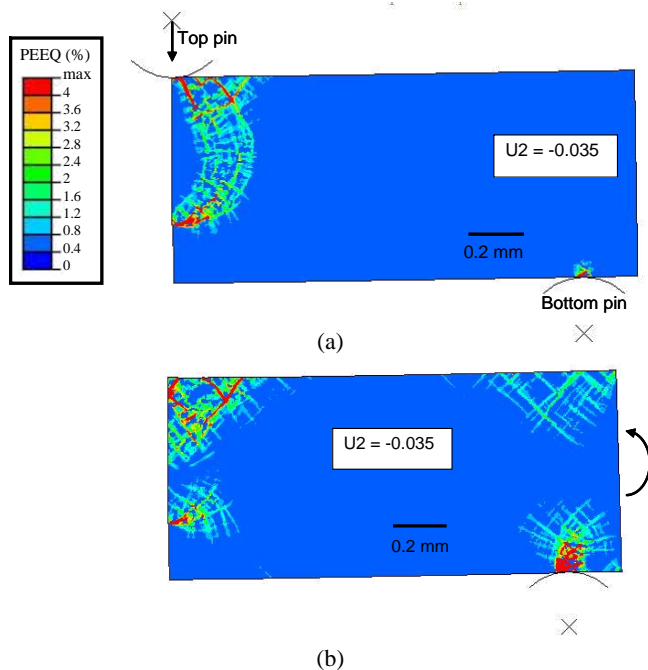


Figure 6. Contour plots of plastic equivalent strain for the microstructure shown in Figure 4b at U2 of 0.035 for (a) pushing top pin and (b) end moment loading configurations.

- Dimiduk, D.M. and Perepezko, J.H. 2003. Mo-Si-B Alloys: Developing a Revolutionary Turbine-Engine Material. MRS Bulletin. 28, 639-645.
- Ito, K., Ihara, K., Tanaka, K., Fujikura, M. and Yamaguchi, M. 2001. Physical and mechanical properties of single crystals of the T2 phase in Mo-Si-B system. Intermetallics. 6, 591-602.